applied sciences

MDPI

Article

Analysis of Pulses Bandwidth and Spectral Resolution in Femtosecond Stimulated Raman Scattering Microscopy

Luigi Sirleto [1], Rajeev Ranjan [1,2] and Maria Antonietta Ferrara [1,*]

[1] National Research Council (CNR), Institute of Applied Sciences and Intelligent Systems, Via Pietro Castellino 111, 80131 Naples, Italy; luigi.sirleto@cnr.it (L.S.); rajeev.ranjan@iit.it (R.R.)
[2] CHT @Erzelli Nanoscopy Istituto Italiano di Tecnologia, 16152 Genova, Italy
* Correspondence: antonella.ferrara@na.isasi.cnr.it

Featured Application: Stimulated Raman microscopy, based on two femtosecond pulsed lasers and with a spectral resolution of about 56 cm^{-1}, is demonstrated to be sufficient in order to distinguish protein and lipid bands in the C-H region.

Abstract: In the last decade, stimulated Raman scattering (SRS) imaging has been demonstrated to be a powerful method for label-free, non-invasive mapping of individual species distributions in a multicomponent system. This is due to the chemical selectivity of SRS techniques and the linear dependence of SRS signals on the individual species concentrations. However, even if significant efforts have been made to improve spectroscopic coherent Raman imaging technology, what is the best way to resolve overlapped Raman bands in biological samples is still an open question. In this framework, spectral resolution, i.e., the ability to distinguish closely lying resonances, is the crucial point. Therefore, in this paper, the interplay among pump and Stokes bandwidths, the degree of chirp-matching and the spectral resolution of femtosecond stimulated Raman scattering microscopy are experimentally investigated and the separation of protein and lipid bands in the C-H region, which are of great interest in biochemical studies, is, in principle, demonstrated.

Keywords: stimulated Raman microscopy; pulsed source; laser pulse bandwidths; laser chirping; spectral resolution

Citation: Sirleto, L.; Ranjan, R.; Ferrara, M.A. Analysis of Pulses Bandwidth and Spectral Resolution in Femtosecond Stimulated Raman Scattering Microscopy. *Appl. Sci.* **2021**, *11*, 3903. https://doi.org/10.3390/app11093903

Academic Editors: Bernhard Wilhelm Roth and Andrés Márquez

Received: 15 March 2021
Accepted: 23 April 2021
Published: 26 April 2021

1. Introduction

Over the past ten years, stimulated Raman scattering (SRS) microscopy has been investigated in nanophotonics [1–4] as well as in biophotonics as an analytical, label-free, non-invasive technique with unique cellular and tissue imaging capabilities [5–8]. As almost all the biomolecules contain carbon and hydrogen, the CH-stretching (2800–3100 cm^{-1}) region of Raman spectra of biomolecules is the most used in SRS microscopy. The two Raman bands typically investigated are CH_2, near to 2845, and CH_3, near to 2930 cm^{-1}, corresponding to lipids and proteins, respectively. Due to their large spectral shapes (about 100 cm^{-1}) and the difference between peaks of 95 cm^{-1}, the CH_2 and CH_3 are partially overlapped. Moreover, in the C-H region, the SRS signal level is high because the density of CH bonds is high, while the SRS molecular specificity is assumed to be low.

Typically, SRS microscopy is implemented by using two Fourier transform-limited (FTL) tunable picosecond (ps) laser sources with a high spectral resolution (≈10 cm^{-1}), helpful in the region of interest (i.e., the fingerprint region: 800 ÷ 1800 cm^{-1}), where Raman peaks are narrow, nearly spaced, and could be packed [8]. However, when ps laser pulses are used to implement an SRS microscope, an equally fruitful imaging in carbon–hydrogen (C-H) stretching is achieved. The drawback is that ps pulses show a low peak intensity, thus needing high laser power for imaging [5–8]. In the last decade, an improvement of about one order of magnitude of the SRS signal has been demonstrated when ps pulses are replaced with femtosecond (fs) pulses [9]. This improvement is due

to a higher peak intensity; thus, higher signal-to-noise ratio (SNR) can be obtained when temporally shorter pulses are used than narrowband, picosecond pulses with an unchanged optical power. However, when ultra-fast sources are used, a low spectral selectivity is obtained and multi-band excitation can occur, not allowing, in principle, the separation of some bands of particular interest in biology, such as those of lipids and proteins as discussed previously. To solve this issue, a number of methods for SRS multicolor imaging, based on broadband femtosecond pulses, have been developed. Among them, frequency tuning [10], multiplexing [11,12] and spectral focusing [13–16] implementations have been studied and reported in the literature.

It is well known that the light pulse is considered transform-limited when the angular frequency is constant and equals the central angular frequency $\omega(t) = \omega_0$. On the other hand, the chirp of an optical pulse is generally understood as the time dependence of its instantaneous frequency; thus, a chirped pulse having a carrier frequency ω_0 at time t shows an instantaneous central frequency $\omega(t)$ that depends on the linear chirp parameter β by the equation: $\omega(t) = \omega_0 + 2\beta t$ [17]. In detail, a down-chirp (up-chirp) means that the instantaneous frequency decreases (increases) with time. A pulse can gain a chirp, for example, through propagation in a transparent medium due to the effects of chromatic dispersion and nonlinearities. Indeed, due to its wide spectral width and to group velocity dispersion, optical pulse propagating in a transparent medium undergoes a phase distortion inducing an increase in its duration with a different laser frequency distribution in time, as reported in Figure 1. In particular, the time–bandwidth product $\Delta\omega_0 \cdot \tau_0 = 4 \ln 2 \approx 2.77$ corresponds to the area of the ellipse on the left in Figure 1 and it is the bandwidth of an FTL laser pulse. As a result of the chirp, laser pulses can undergo a temporal stretch and the final pulse duration is $\tau = F\tau_0$, where τ_0 is the FTL pulse duration and F is the stretching factor; at the same time, the instantaneous spectral bandwidth becomes narrower than the FTL spectral bandwidth by a factor of $1/F$ [18]. With the relation $\Delta\omega \cdot \tau = 2.77$ also being applicable to the chirped pulse width τ and to the instantaneous bandwidth $\Delta\omega$ of the pulse, the duration broadening leads to a decrease in the instantaneous bandwidth by the stretching factor, whereas the whole bandwidth $\Delta\omega_0$ is left unchanged [19], as depicted in Figure 1.

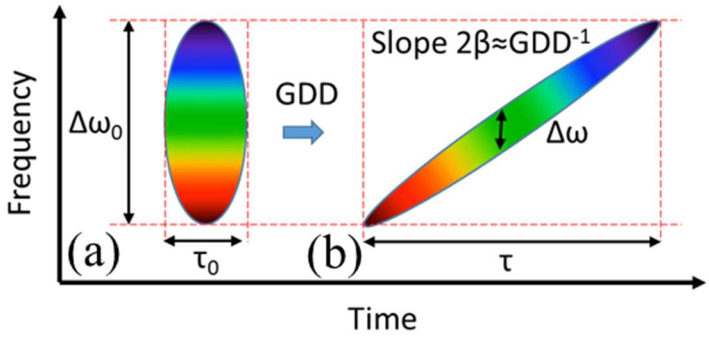

Figure 1. Time-bandwidth distribution for (**a**) Fourier-transform limited laser pulse and (**b**) the same laser pulse that is linearly chirped.

In order to enhance spectral resolution in SRS microscopy based on fs laser pulses, an option is to force a quadratic spectral phase variation. By equally chirping pump and Stokes beams with an energy spacing corresponding to the Raman line, it is possible to generate a constant instantaneous frequency difference (IFD, $\Omega = \omega_p - \omega_s$) that spectrally focuses the excitation energy into a single resonance. We note that the bandwidth $\delta\Omega$, which ultimately determines the SRS spectral resolution, in the limiting case can simulate the ps SRS system. This method is known as spectral focusing (SF) [13–16]. Nevertheless, the great disadvantage related to this approach is the large amount of parameters that should be taken into account in the selection and alignment of the optics to obtain the chirp-matching condition. Moreover, since the operative conditions can be altered by

fluctuations in the pump and Stokes wavelengths together with the dispersion in the microscope, perfect chirp-matching is difficult to maintain. For these reasons, the resulting spectral resolution of SF-SRS setups is often worse than theoretically predicted [13–16].

The comparison among FTL, equally and differently chirped laser sources is shown in Figure 2. In the spectral focusing, when the pump and Stokes pulses are "chirp-matched", the bandwidth of IFD is lower than the total bandwidths of the transform-limited pulses, leading to an improvement of the spectral resolution, as reported in Figure 2b. On the other hand, when the chirp-matching condition is not met, the bandwidth of the IFD signal is broader, and, as a consequence, the spectral resolution is poorer with respect to the chirp matched case (see Figure 2c). Interestingly, spectral resolution for differently chirped lasers is better than FTL laser sources [19].

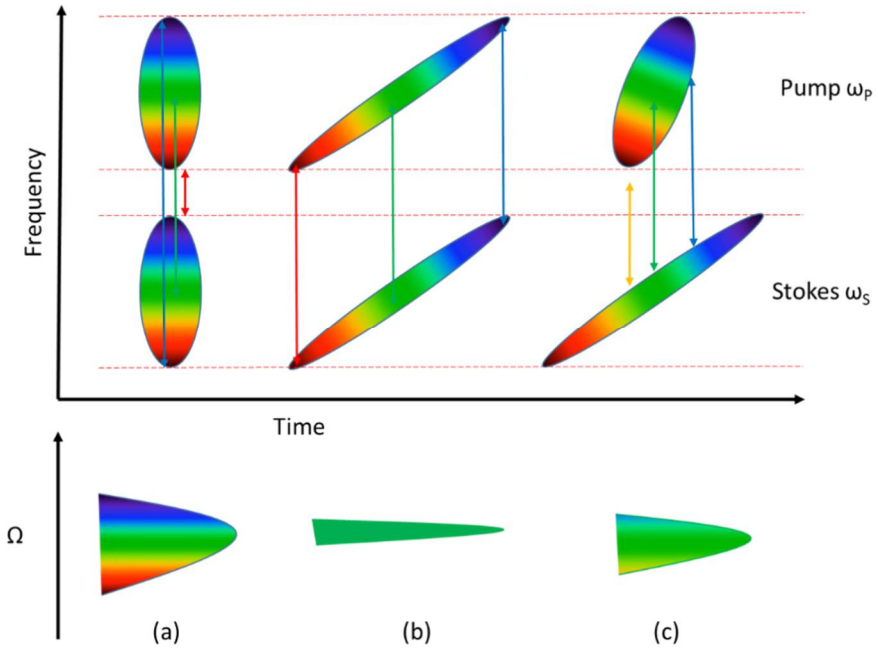

Figure 2. Coherent Raman excitation with (**a**) FTL laser pulses, (**b**) laser pulses with the same chirp, (**c**) laser pulses with different chirps. Ω is the vibration frequency given by $\Omega = \omega_p - \omega_s$.

For microscopy, both contrast imaging and spectral tuning are important to assess the good quality of images. However, in coherent Raman scattering, there is a tradeoff between the best spectral resolution, which is reached with ps sources, and the best ratio of image contrast and signal intensity, which is obtained when the spectral resolution and the width of the Raman lines under observation are almost the same [14]. This condition is satisfied in the case of excitation with both ps pulses, since they match the linewidths in the fingerprint region (5–20 cm^{-1}), and in the case of broader bandwidth femtosecond (fs) pulses, which are considered the ideal excitation for CH stretching vibrations.

We note that the SF approach usually takes advantage by static dispersive elements, such as glass rods, placed into the optical path to stretch both the pump and the Stokes frequencies in time and produce a constant IFD. However, the optical elements embedded in an SRS optical circuitry microscope setup can also change the pulse width. In this paper, taking advantage of the small chirping, introduced by simply propagating the beams through dispersive materials already present in the SRS microscope setup, we examine the spectral correlations and we demonstrate that its value is enough to distinguish protein and lipid bands in the C-H region.

2. Experimental Setup and Methods

Our optical system, not commercially existing and schematically shown in Figure 3, is obtained by integrating a femtosecond-SRS spectroscopy setup [20–22] with a C2 con-

focal Nikon microscope, which consists of an inverted Nikon Ti-eclipse microscope and a scan head. Experimental details of our setup have already been reported in our previous papers [22–25]. Two femtosecond laser sources are involved in this setup: a Ti:Sapphire (Ti:Sa—Chameleon Ultra II—pulse duration = 140 fs, repetition rate = 80 MHz, emission wavelengths range = 680–1080 nm) and a femtosecond synchronized optical parametric oscillator (OPO—Chameleon Compact OPO—pulse duration = 200 fs, repetition rate = 80 MHz, emission wavelengths range = 1000–1600 nm).

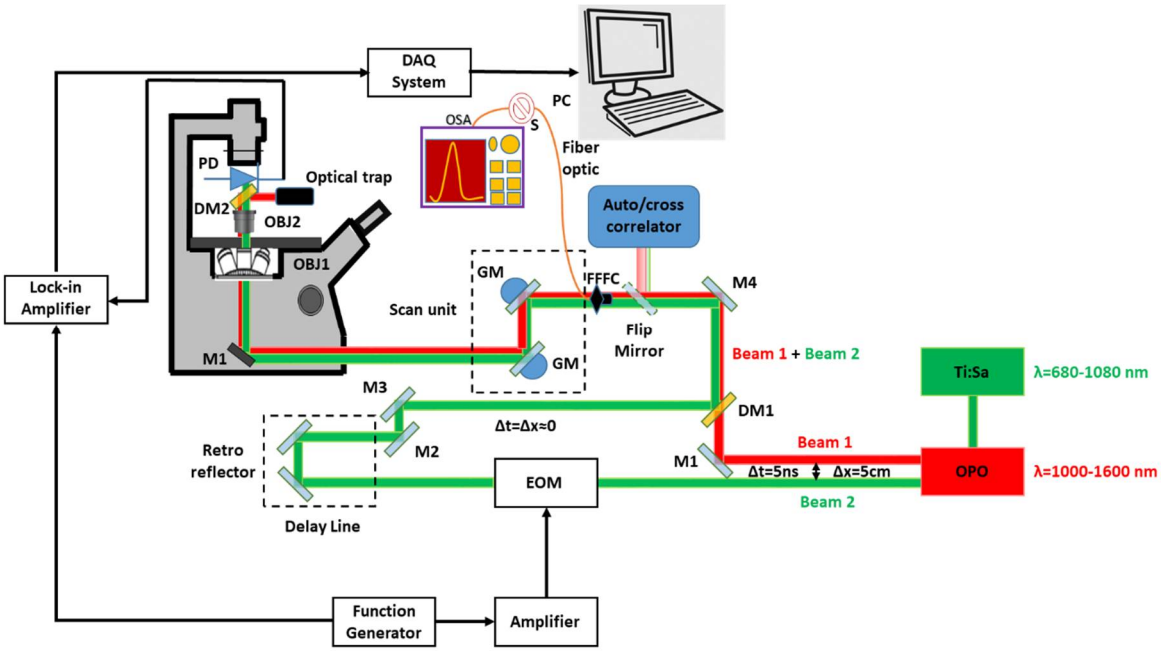

Figure 3. Experimental setup for stimulated Raman scattering imaging. (Ti:Sa): Titanium-Sapphire pulsed laser source; OPO: optical parameter oscillator; M: mirror; EOM: electro-optical modulator; GM: galvo-mirror; DM: dichroic mirror; OBJ: objective lens; PD: photo-detector; FFFC: flip flop fiber coupler; S: multimode optical fiber; OSA: optical spectrum analyzer.

Typically, the temporal characterization of a signal is performed by measuring the correlation between the signal and its duplication. In particular, optical autocorrelation of the field intensity may be used to measure the second-order coherence degree and to assess the duration of short pulses. With this aim, an additional flip-flop mirror has been mounted in-between the mirror M4 and the input of the scan head in our optical architecture to deflect the laser pulse beams directly toward an autocorrelator (pulseCheck 50–A.P.E., Berlin) (see Figure 3); therefore, auto- and cross-correlation of the pulse beam were measured in the optical path just before the laser beam reaches the microscope. In an autocorrelator, the input pulsed beam is divided into two arms of a Michelson interferometer and a delay can be induced in the pulses in one arm with respect to the other one. Both pulses are then overlapped in a non-linear crystal and the generated signal is detected. The pulse duration can be evaluated from the measurement of the time delay and the intensity of the generated signal [26]. The detectable pulse width range is fixed by the delay range, whereas the measurable wavelength range is determined by the detector and the non-linear material. Here, the nonlinear process is the two photons absorption (TPA) and it is measured as a function of the time delay giving the beam autocorrelation function. Auto-correlators based on TPA have some important advantages: (i) a higher sensitivity can be obtained with respect to second harmonic generation (SHG) due to the involvement of fields only at the original frequency, ω, owing to the TPA resonant second-order transition nature; (ii) extremely short pulses can be characterized since TPA can operate in a wide wavelength range not restricted by the narrow phase matching bandwidth; (iii) in TPA, non-linear signal multiplication and detection are combined into one process, leading

to a simplification and a higher efficiency with respect to a two-step process of optical non-linearity followed by linear detection.

The used pulseCheck can be used in two measurement modes: collinear and non-collinear. Collinear, also known as interferometric or fringe-resolved mode, provides further qualitative information on the chirp and central wavelength of the pulse. Regarding non-collinear mode, it allows high dynamic range measurements that are background free [27].

The auto- correlator was used with a pulse width measurement range of (10 fs–12 ps) and it was connected to the PC through USB and by using the APE's Standardized Software Interface, allowing either remote control or integration into automated setups. Therefore, the deflected beam is tuned until the intensity is stabilized and maximized, and then, the pulse is acquired and the data analysis is completed by using the Gaussian fitting curve function *cftool* of MATLAB 2020.

To evaluate the spectral resolution, the exact estimation of the pulses' duration is required. Normally, the full width at half-maximum (FWHM) of the unknown pulse τ_p is proportional to the FWHM of the measured fringe-resolved intensity autocorrelation function τ_{ac}:

$$\tau_{ac} = k \cdot \tau_p \tag{1}$$

where k is the proportionality factor, also known as the deconvolution factor. k differs significantly for different pulse shapes; therefore, to evaluate the pulse width from the intensity autocorrelation requires some previous knowledge of the pulse shape. Typically, the deconvolution factor can be calculated for analytical pulse shapes or computed numerically for complicated pulses; however, for some common pulse shapes, the deconvolution factor is known (k = 1.414 for Gaussian shape, k = 1.543 for sech shape, k = 1 for square shape) [28].

It is well known that the Fourier transformation correlates β, which defines the linear slope of the central frequency, to the group delay dispersion (GDD) applied to the laser pulse as reported in the following [19]:

$$\beta = \frac{2GDD}{\tau_0^4 + 4GDD^2} \approx \frac{1}{2GDD} \; for \; \tau \gg \tau_0 \tag{2}$$

The GDD leads to a stretch of the pulse width, which passes from τ_0 in the case of the FTL pulse to the chirped width τ:

$$\tau = \tau_0 \sqrt{1 + \left(\frac{4 \ln 2 \cdot GDD}{\tau_0^2} \right)^2} \approx 2.77 \frac{|GDD|}{\tau_0} \; for \; \tau \gg \tau_0 \tag{3}$$

From Equations (2) and (3), we found that $\tau \cdot \tau_0 \approx 4 \ln 2 |GDD| \approx 2 \ln 2 / |\beta|$; this product is considered a direct measure of the chirp parameter β for $\tau \gg \tau_0$ [19]. We note that two chirped pulses have the same slope only if the resultant products $\tau \cdot \tau_0$ are equal.

Information obtained by autocorrelation measurements allows us to monitor the pulse duration and chirp of the laser beam, which are very important parameters to optimize the non-linear interaction in microscopy. Moreover, considering that SRS is a two-pulse technique, its spectral resolution is not defined by the spectrum of the individual exciting pulses but by the spectrum of their temporal interference. Consequently, cross-correlation characterization is equally important for providing information about the entire system; in particular, the FWHM of pump and probe beams' cross-correlation allows us to evaluate the experimental spectral bandwidth [29]. Typically, SF is obtained by equally chirping the pump and the Stokes pulses by using glass elements of known group-velocity dispersion without significant intensity losses [30]. As a general rule, the spectral resolution is restricted both by the level to which the pulses are chirped and by the similarity of these chirps. A better spectral resolution can be obtained when the pump and Stokes pulses with

larger bandwidths are chirp-matched. In the case of transform limited laser pulses, the spectral resolution can be calculated by the formula [19]:

$$\Delta\tilde{\nu} = \frac{2\ln 2}{\pi c}\sqrt{2\left(\tau_p^{-2} + \tau_S^{-2}\right)} = 20.8\ \text{ps}\cdot\text{cm}^{-1}\sqrt{\tau_p^{-2} + \tau_S^{-2}} \quad (4)$$

and in the case of our fs laser sources its evaluated value is of 181 cm^{-1}. In order to carry out cross-correlation between Ti:Sa and OPO, both sources are focused inside the TPA detector, then by inserting an optical delay line (Newport MOD MILS200CC) between the Ti:Sa and the microscope, we introduce an optical delay in the Ti:Sa beam; at each step of the delay line, the signal is acquired.

Finally, to have a complete characterization of the pulsed sources used in our SRS microscope, we have carried out laser spectra measurement by adding a flip flop fiber coupler (FFFC in Figure 3) in the optical setup without disturbing it, and the deflected beam is coupled in an optical spectrum analyzer (OSA—Ando AQ6317C) by a multimode optical fiber S, which is mounted after the flip/flop mirror. In Figure 3, the setup used integrated with the described system for complete characterization of the pulsed laser sources is reported.

3. Results and Discussion

Autocorrelation characterizations of the pulsed laser beams were examined using the aforementioned autocorrelator. The Ti:Sa and OPO laser emission wavelengths were fixed at 811 nm and at 1074 nm, respectively. The collected autocorrelation function of the Ti:Sa and OPO is reported in Figure 4a,b, respectively. As can be seen in these figures, the pulses emitted by the lasers show a Gaussian-like distribution, as expected. Therefore, with the aim to evaluate the pulse width value, both the autocorrelation traces were Gaussian-fitted as displayed in Figure 4a,b, and the corresponding FWHM of the Gaussian curves was calculated to be about 341 fs and 357 fs for Ti:Sa and OPO, respectively. Since the pulse follows a Gaussian line shape and considering Equation (1), the factor of 1.414 was applied to our evaluation, leading to an estimation of the pulses' width duration at the input of the microscope of about τ = 241 fs for Ti:Sa and τ = 253 fs for OPO, respectively. Thus, a small broadening of OPO was observed, while a major one was retrieved for Ti:Sa. These broadenings are related to the dispersion arising during propagation through several optical elements along the beams' path; in particular, the higher widening observed for Ti:Sa can be explained considering that in its optical path a Pockels cell is employed. In Table 1, the features of the two lasers and results of their autocorrelation measurements are summarized.

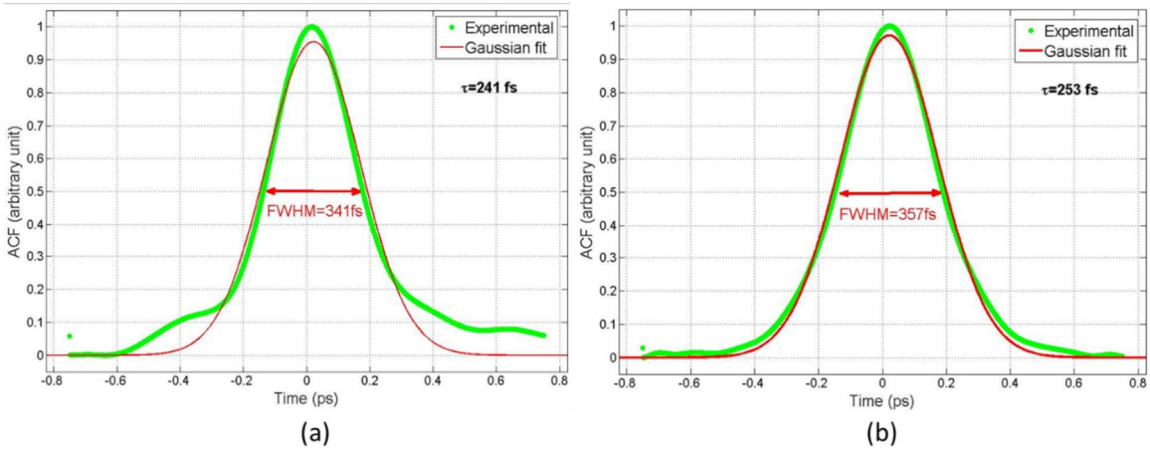

Figure 4. Autocorrelation trace of the pulsed laser sources (**a**) Ti:Sa and (**b**) OPO, respectively. Results of the Gaussian fit are also reported.

Table 1. Pulsed laser sources properties.

Laser Source	Wavelength Range [nm]	Pulse Duration [fs]	Repetition Rate [MHz]	Widened Pulse Duration [fs]
Ti:Sa	740–880	140	80	241
OPO	1000–1600	200	80	253

The second order group velocity dispersion can be evaluated for each pulsed source by applying Equations (2) and (3). The obtained values are GDD = 9905 fs^2 and GDD = 11,177 fs^2 for Ti:Sa and OPO, respectively. In our case, pulses were not equally chirped.

To complete the single beam characterization, the laser spectra were acquired by an optical spectrum analyzer and results are shown in Figure 5, when Ti:Sa is tuned to 811 nm and OPO to 1074 nm, respectively. The resultant bandwidths are approximately the same for both pulsed laser sources and were of about 6.1 nm.

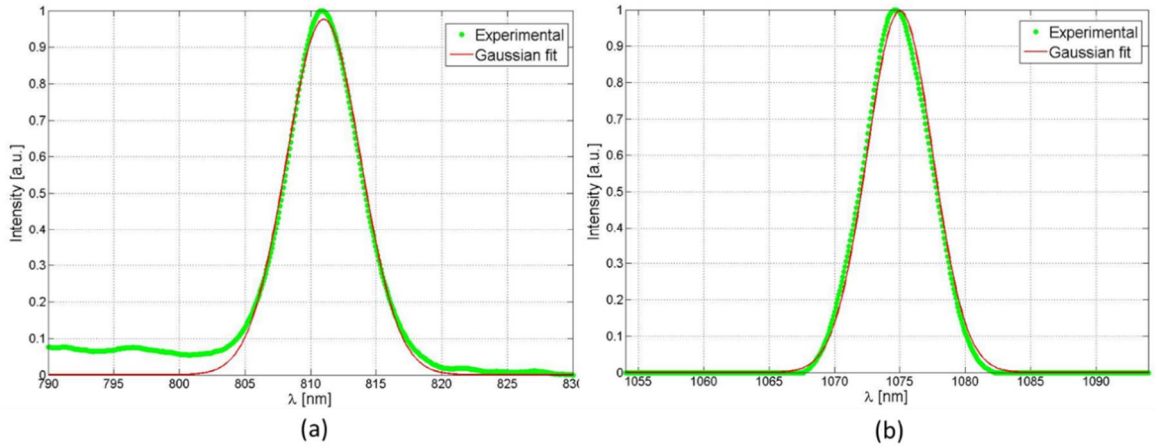

Figure 5. Optical spectra of the pulsed laser sources (**a**) Ti:Sa and (**b**) OPO, respectively. Results of the Gaussian fit are also reported.

The measured FWHM of Ti:Sa and OPO cross-correlation was 371 fs; since the convolution of two Gaussian functions is another a Gaussian function [31], Equation (1) can also be applied when cross-correlation measurements are performed, leading to a pulse duration of 262 fs (see Figure 6). Thus, the obtained experimental spectral bandwidth, which is given by the FWHM of cross-correlation in the frequency domain, was of 56 cm^{-1}.

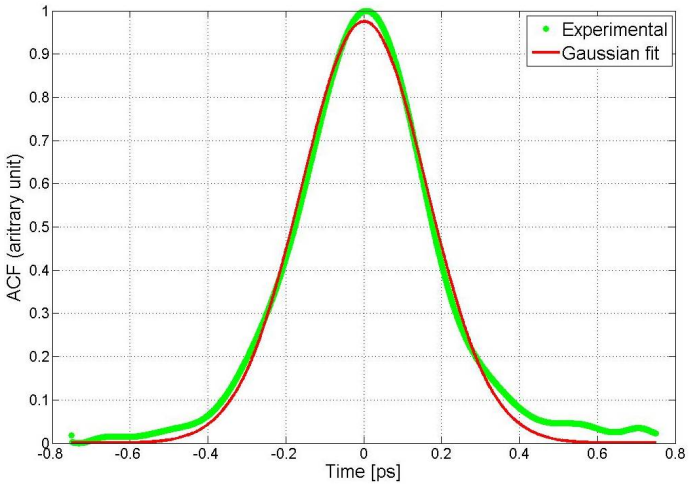

Figure 6. Cross-correlation measure and its Gaussian fit.

The retrieved spectral resolution is very useful in biological sample imaging when both lipid and protein bands need to be investigated by SRS microscopy by simply regulating the frequency either of the pump or the Stokes beams in successive scans. The corresponding two stretching signals are CH_2 (2845 cm^{-1}) and CH_3 (2940 cm^{-1}), respectively; thus, these bands can be collected by choosing one Raman shift at a time, allowing the imaging of the map distributions of the lipid and protein on the same field of the sample. Therefore, since our experimental spectral bandwidth was of 56 cm^{-1}, when we set the laser beams to excite the 2845 cm^{-1} lipid band, we are exciting from (FWHM) 2817 to 2873 cm^{-1}; in the same way, when we set the laser beams to the protein band at 2940 cm^{-1}, effectively we excite the range 2912–2968 cm^{-1} (FWHM). In Figure 7, the spectral bandwidth derived by the chirping of the pulses (56 cm^{-1}—continuous lines) and two simulated Raman bands with two peaks at a distance of 95 cm^{-1} with a width of about 100 cm^{-1} (red circles and green diamonds) are illustrated.

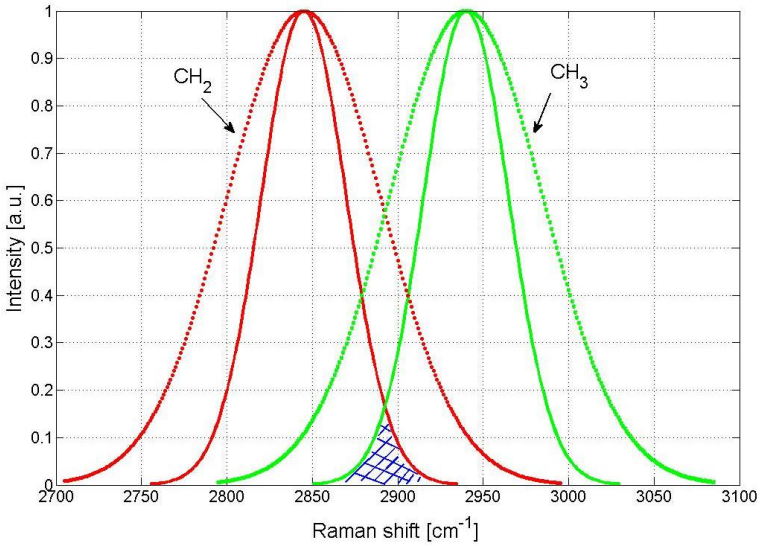

Figure 7. Raman bands for CH_2 (2845 cm^{-1}, red circles) and CH_3 (2940 cm^{-1}, green diamonds). Continuous lines are obtained considering the Ti:Sa and OPO cross-correlation reported in Figure 6 at the input of the microscope (i.e., 262 fs). Blue lines highlight the overlap area between two excited bandwidths.

The overlap between two excited bandwidths is highlighted with blue lines; however, the contribution to the Raman signal from this region can be neglected considering that the intensities are lower than FWHM values and, therefore, they can be considered under the threshold. Thus, we can conclude that, using 56 cm^{-1} chirped pulses, the 2845 cm^{-1} channel is essentially related to the lipid signal and the 2940 cm^{-1} channel is principally due to protein content. Definitely, considering the retrieved experimental spectral resolution (about 56 cm^{-1}) that is lower than the Raman band of lipids and proteins (about 100 cm^{-1}) and since the overlap region, obtained when lipids and proteins are sequentially excited, can be considered negligible, our SRS microscope is suitable to image molecular specificity such as lipids (CH_2) and proteins (CH_3) in the C-H region, as already demonstrated in our previous paper [23].

4. Conclusions

In SRS microscopy, the trade-off between high selectivity offered by picosecond pulses and high SRS signal obtained by using femtosecond pulses is still an open question and it is widely investigated. In particular, for biological application, there is interest in label-free imaging both the lipid and protein distribution. Unfortunately, the Raman bands of these two components are very close, thus ps pulses are required; however, the protein content could be low, leading to very weak Raman signals, so fs pulses would be appropriate.

In this paper, in order to overcome the drawback of spectral focusing, an alternative method is proposed. Its basic idea is to avoid adding optical elements in the SRS microscopy optical setup and to take advantage of chirping, introduced by simply propagating the beams through dispersive materials already present in the SRS microscope. The pros are that no additional optical elements have to be introduced in the experimental setup, giving the great advantage of a more simple and cheap setup; the cons are that the spectral resolution is fixed. However, in our setup, an experimental value of 56 cm^{-1} for spectral resolution is measured by cross-correlation techniques, and molecular specificity is demonstrated for lipids and proteins in the C-H region.

Moreover, the spectral resolution was measured before the microscope, and this means that a significant further chirping of laser pulses is expected due to the propagation of the pulsed beams inside the scan head and of the microscope objective, leading to an additional improvement in spectral resolution. Definitely, our method has the merit to maintain the benefits of femtosecond pulses, i.e., an improvement in sensitivity with respect to ps pulses, while preserving in the C-H region of Raman spectra of biomolecules an adequate spectral resolution.

Author Contributions: Conceptualization, methodology, investigation, validation, data analysis, writing—original draft preparation: M.A.F., R.R. and L.S. All authors have read and agreed to the published version of the manuscript.

Funding: This research received no external funding.

Data Availability Statement: The datasets generated during and/or analyzed during the current study are available from the corresponding author on reasonable request.

Acknowledgments: The authors would like to thank M. Indolfi and V. Tufano (ISASI-CNR) for their precious and constant technical assistance.

Conflicts of Interest: The authors declare no conflict of interest. The funders had no role in the design of the study; in the collection, analyses, or interpretation of data; in the writing of the manuscript, or in the decision to publish the results.

References

1. Sirleto, L.; Ferrara, M.A.; Nikitin, T.; Novikov, S.; Khriachtchev, L. Giant Raman gain in silicon nanocrystals. *Nat. Commun.* **2012**, *3*, 1220. [CrossRef] [PubMed]
2. Sirleto, L.; Vergara, A.; Ferrara, M.A. Advances in stimulated Raman scattering in nanostructures. *Adv. Opt. Photon* **2017**, *9*, 169–217. [CrossRef]
3. Ferrara, M.; Sirleto, L.; Nicotra, G.; Spinella, C.; Rendina, I. Enhanced gain coefficient in Raman amplifier based on silicon nanocomposites. *Photon Nanostruct. Fundam. Appl.* **2011**, *9*, 1–7. [CrossRef]
4. Sirleto, L.; Aronne, A.; Gioffrè, M.; Fanelli, E.; Righini, G.C.; Pernice, P.; Vergara, A. Compositional and thermal treatment effects on Raman gain and bandwidth in nanostructured silica based glasses. *Opt. Mater.* **2013**, *36*, 408–413. [CrossRef]
5. Freudiger, C.W.; Min, W.; Saar, B.G.; Lu, S.; Holtom, G.R.; He, C.; Tsai, J.C.; Kang, J.X.; Xie, X.S. Label-Free Biomedical Imaging with High Sensitivity by Stimulated Raman Scattering Microscopy. *Science* **2008**, *322*, 1857–1861. [CrossRef] [PubMed]
6. Cheng, J.-X.; Xie, X.S. Vibrational spectroscopic imaging of living systems: An emerging platform for biology and medicine. *Science* **2015**, *350*, aaa8870. [CrossRef]
7. Camp, C.H., Jr.; Cicerone, M.T. Chemically sensitive bioimaging with coherent Raman scattering. *Nat. Photon* **2015**, *9*, 295–305. [CrossRef]
8. Zumbusch, A.; Langbein, W.; Borri, P. Nonlinear vibrational microscopy applied to lipid biology. *Prog. Lipid Res.* **2013**, *52*, 615–632. [CrossRef]
9. Zhang, D.; Slipchenko, M.N.; Cheng, J.-X. Highly Sensitive Vibrational Imaging by Femtosecond Pulse Stimulated Raman Loss. *J. Phys. Chem. Lett.* **2011**, *2*, 1248–1253. [CrossRef]
10. Steinle, T.; Kumar, V.; Floess, M.; Steinmann, A.; Marangoni, M.; Koch, C.; Wege, C.; Cerullo, G.; Giessen, H. Synchroniza-tion-free all-solid-state laser system for stimulated Raman scattering microscopy. *Light Sci. Appl.* **2016**, *5*, e16149. [CrossRef] [PubMed]
11. Fu, D.; Lu, F.K.; Zhang, X.; Freudiger, C.W.; Pernik, D.R.; Holtrom, G.; Xie, X.S. Quantitative chemical imaging with mul-tiplex stimulated Raman scattering microscopy. *J. Am. Chem. Soc.* **2012**, *134*, 3623–3626. [CrossRef]
12. Liao, C.-S.; Wang, P.; Wang, P.; Li, J.; Lee, H.J.; Eakins, G.; Cheng, J.-X. Spectrometer-free vibrational imaging by retrieving stimulated Raman signal from highly scattered photons. *Sci. Adv.* **2015**, *1*, e1500738. [CrossRef]

13. Fu, D.; Holtom, G.; Freudiger, C.; Zhang, X.; Xie, X.S. Hyperspectral Imaging with Stimulated Raman Scattering by Chirped Femtosecond Lasers. *J. Phys. Chem. B* **2013**, *117*, 4634–4640. [CrossRef]
14. Brückner, L.; Buckup, T.; Motzkus, M. Exploring the potential of tailored spectral focusing. *J. Opt. Soc. Am. B* **2016**, *33*, 1482–1491. [CrossRef]
15. Pegoraro, A.F.; Ridsdale, A.; Moffatt, D.J.; Jia, Y.W.; Pezacki, J.P.; Stolow, A. Optimally chirped multimodal CARS micros-copy based on a single Ti:sapphire oscillator. *Opt. Express* **2009**, *17*, 2984–2996. [CrossRef]
16. Rocha-Mendoza, I.; Langbein, W.; Borri, P. Coherent anti-Stokes Raman microspectroscopy using spectral focusing with glass dispersion. *Appl. Phys. Lett.* **2008**, *93*, 201103. [CrossRef]
17. Hirlimann, C. Pulsed Optics. In *Femtosecond Laser Pulses Principle and Experiments*, 2nd ed.; Rullier, C., Ed.; Springer: New York, NY, USA, 2005; pp. 25–56.
18. Beier, H.T.; Noojin, G.D.; Rockwell, B.A. Stimulated Raman scattering using a single femtosecond oscillator with flexibility for imaging and spectral applications. *Opt. Express* **2011**, *19*, 18885–18892. [CrossRef] [PubMed]
19. Mohseni, M.; Polzer, C.; Hellerer, T. Resolution of spectral focusing in coherent Raman imaging. *Opt. Express* **2018**, *26*, 10230–10241. [CrossRef] [PubMed]
20. Ranjan, R.; D'Arco, A.; Ferrara, M.A.; Indolfi, M.; Larobina, M.; Sirleto, L. Integration of stimulated Raman gain and stimu-lated Raman losses detection modes in a single nonlinear microscope. *Opt. Express* **2018**, *26*, 26317–26326. [CrossRef]
21. D'Arco, A.; Ferrara, M.A.; Indolfi, M.; Tufano, V.; Sirleto, L. Label-free imaging of small lipid droplets by femtosec-ond-stimulated Raman scattering microscopy. *J. Nonlinear Opt. Phys. Mater.* **2017**, *26*, 1750052. [CrossRef]
22. Ranjan, R.; Indolfi, M.; Ferrara, M.A.; Sirleto, L. Implementation of a Nonlinear Microscope Based on Stimulated Raman Scattering. *J. Vis. Exp.* **2019**, *2019*, e59614. [CrossRef]
23. Ferrara, M.A.; Filograna, A.; Ranjan, R.; Corda, D.; Valente, C.; Sirleto, L. Three-dimensional label-free imaging throughout adipocyte differentiation by stimulated Raman microscopy. *PLoS ONE* **2019**, *14*, e0216811. [CrossRef]
24. Ranjan, R.; Ferrara, M.; Filograna, A.; Valente, C.; Sirleto, L. Femtosecond Stimulated Raman microscopy: Home-built realization and a case study of biological imaging. *J. Instrum.* **2019**, *14*, P09008. [CrossRef]
25. D'Arco, A.; Brancati, N.; Ferrara, M.A.; Indolfi, M.; Frucci, M.; Sirleto, L. Subcellular chemical and morphological analysis by stimulated Raman scattering microscopy and image analysis techniques. *Biomed. Opt. Express* **2016**, *7*, 1853–1864. [CrossRef] [PubMed]
26. Piazza, V.; De Vito, G.; Farrokhtakin, E.; Ciofani, G.; Mattoli, V. Femtosecond-Laser-Pulse Characterization and Optimization for CARS Microscopy. *PLoS ONE* **2016**, *11*, e0156371. [CrossRef]
27. Berlin, A.P.E. Available online: https://www.ape-berlin.de/en/autocorrelator/ (accessed on 10 February 2021).
28. Chen, J.; Xia, W.; Wang, M. Characteristic measurement for femtosecond laser pulses using a GaAs PIN photodiode as a two-photon photovoltaic receiver. *J. Appl. Phys.* **2017**, *121*, 223103. [CrossRef]
29. Ito, T.; Obara, Y.; Misawa, K. Single-beam phase-modulated stimulated Raman scattering microscopy with spectrally focused detection. *J. Opt. Soc. Am. B* **2017**, *34*, 1004. [CrossRef]
30. Andresen, E.R.; Berto, P.; Rigneault, H. Stimulated Raman scattering microscopy by spectral focusing and fiber-generated soliton as Stokes pulse. *Opt. Lett.* **2011**, *36*, 2387–2389. [CrossRef]
31. Getreuer, P. A Survey of Gaussian Convolution Algorithms. *Image Process. Line* **2013**, *3*, 286–310. [CrossRef]